Toward the prediction of low-speed fan noise

**By S. Moreau, M. Henner †, D. Casalino ‡,
J. Gullbrand ¶, G. Iaccarino AND M. Wang ‖**

A first attempt at computing the complete noise spectrum of a low-speed fan is presented. The tonal noise prediction relies on the Ffowcs Williams-Hawkings acoustic analogy with the pressure fluctuations on the blades computed from detailed Unsteady Reynolds-Averaged Navier-Stokes simulations (URANS). The broadband noise calculation relies on a strip theory, which describes the fan blade as a series of independent airfoils in translation at the local relative velocity. The noise sources are assumed to be uncorrelated, and similar to that of a stationary airfoil in the jet flow of an anechoic wind tunnel. The overall agreement of the combined acoustic spectra with the measurements on an automotive engine cooling module suggests that the URANS can yield accurate noise sources for tonal noise and that two broadband noise mechanisms co-exist: the turbulence-interaction noise at low and intermediate frequencies, and the trailing-edge noise at high frequencies beyond 4 kHz.

1. Introduction

Noise nuisance is an increasing environmental concern in large urban areas and a differentiation factor in many industrial sectors, e.g., daily appliances, aerospace, automotive and computers. For instance, in the design process of a new automotive engine cooling fan system, one major requirement that has to be fulfilled by Valeo is a minimum noise configuration for a given duty point of cooling modules with increasing heat rejection. Similarly, in the design of more powerful electronic chips, the cooling requirements are increasing. The cooling requirements of a computer must take a balanced approach to cooling and acoustics for optimal user experience. Accurate noise simulation of low-speed fans and a correlation of the noise sources with their physical topology and environment are therefore increasingly needed.

As Caro & Moreau (2000) noted, the noise radiated by these low-speed axial fans is tonal and broadband, both contributions are equally important in most configurations. The broadband noise can be even more important in other low-speed axial fans, such as the propellers of air conditioning units or large wind turbines (Hubbard & Shepherd 1991). Several different noise mechanisms can generate high tones in these rotating machines (Huang 2003). Because of their low-speed (Mach number $M \ll 1$), the mean fan load will not contribute, but any unsteady fan load will create tonal noise. For instance, the non-uniform inlet flow conditions will cause variations of the incidence angle of the airflow on the blades and consequently wall pressure fluctuations. Depending on the distance from the fan blade trailing-edge and the support struts or stator vanes, two additional tonal noise sources may arise: on the one hand, the wakes shed by the rotors

† Valeo Thermal Systems, France
‡ CIRA, Italy
¶ Systems Technology Lab, Intel, USA
‖ University of Notre Dame, USA

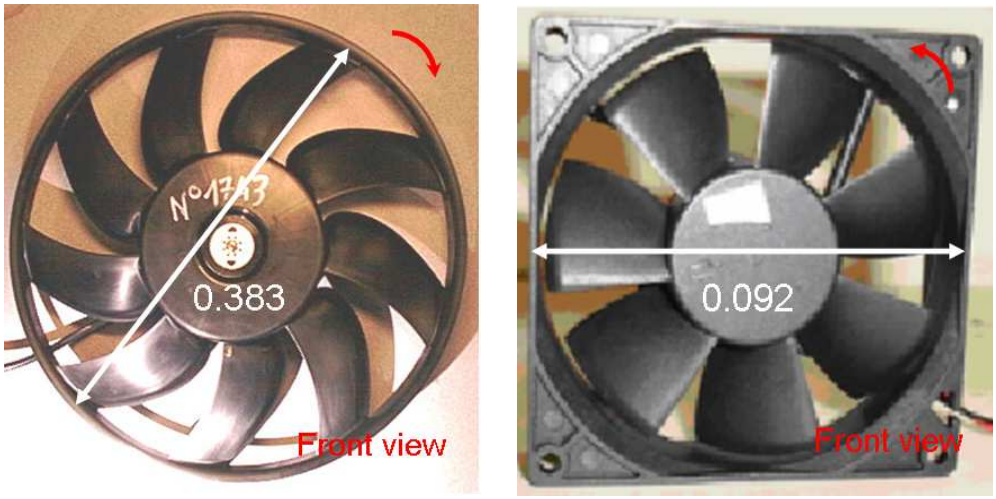

(a) Automotive engine cooling fan (b) Electronic cooling fan

FIGURE 1. *Selected low-speed cooling fan systems.*

will periodically create a variation of load on the stationary parts (rotor-stator wake interaction); on the other hand, the flow disturbance induced by the stator will trigger rotor wall pressure fluctuations at its trailing-edge if the rotor-stator distance is small enough (rotor-stator potential interaction). Note that these two sources are located on the other element when the stator is placed before the rotor. Finally, additional obstacles immediately downstream of the fan system may create potential unsteadiness on the stationary parts and even on the rotor, if strong enough. Similarly, several competing mechanisms may contribute to the broadband noise. A first important element is the fan self-noise generated at the blade trailing-edge. As quoted by Wright (1976), trailing-edge noise always exists and provides the minimum noise that a spinning fan would produce free of any upstream, downstream, and tip flow/blade interactions. Another major contribution is the noise due to upstream turbulence impinging on the leading-edge, referred to here as leading-edge noise. It originates from the ingestion of large vortical structures such as the elongated ground turbulence ingested by a helicopter tail-rotor, or small scale turbulence shed for instance by the heat exchanger core of the automotive puller module.

The next section describes the industrial fan systems of Valeo and Delta Electronics that are considered in the present study. Steady and unsteady Reynolds-Averaged Navier-Stokes (RANS) simulations of the three-dimensinal flow around these fan systems are then presented. They provide the deterministic noise sources for a time-domain numerical prediction of the far field tonal noise based on the Ffowcs Williams-Hawkings (FWH) acoustic analogy. Direct predictions of the broadband turbulent wall pressure fluctuations for the entire 3-D fan blades are currently unavailable. An alternative method is thus explored. The broadband noise prediction relies on semi-analytical models for trailing-edge noise and turbulence-interaction noise applied by strips along the blade span, with inputs from detailed LES for the Valeo Controlled Diffusion (CD) airfoil properly rescaled to account for the proper local fan flow properties. The numerical results are compared to the experimental data collected in the Valeo semi-anechoic chambers.

2. Industrial background

Two typical automotive engine cooling fan systems have been selected in the present study. The fan topologies belong to the ultra compact fan range recently developed by Valeo. Both have 9 asymmetric blades and the same radial stacking and planform (same chord distribution and sweep). The first fan has a 320 mm diameter ($2R_f$); the other one has a 380 mm diameter. They have homothetic hub and rotating ring diameters. Only the stagger angles and aerodynamic profiles vary slightly in the tip region because of different operating conditions. The larger fan system rotates with a speed Ω of 2500 rpm for a flow rate of 2500 m^3/h at peak efficiency. The smaller fan system (Fig. 1a) spins at 3000 rpm for a flow rate of 1700 m^3/h at peak efficiency. This corresponds to a maximum Mach number of 0.15 and Reynolds numbers based on the chord length ranging from 6×10^4 to 1.8×10^5. The electronic cooling fan is a typical 92 mm fan with 7 symmetric blades (Fig. 1b). This particular fan is used as a chassis fan and not for cooling the CPU itself. Its maximum flow rate is approximately 90 m^3/h for a rotation of 3000 rpm. This yields a maximum Mach number of 0.09 and Reynolds numbers based on the chord length at approximately 5×10^4. Consequently the flow through both sets of rotating machines is transitional and essentially incompressible.

3. Flow simulations

3.1. *Grid topology and boundary conditions*

To limit the numerical model size, only a single blade passage is meshed and simulated, and consequently a symmetric blade distribution is assumed in all flow simulations for both applications.

The grid topology for the automotive fan corresponds to the automatic multi-block-structured grid template used for accurately simulating the Valeo fan test rigs: an inlet box accounting for an upstream plenum, a fan mounted on a wall with a constant tip clearance, and an outlet box representing the laboratory. The central block includes the actual blade geometry and fan tip clearance configuration. Downstream, the motor or torque meter blockage is accounted for. Only the swirling effect of the ribs within the fan hub is neglected. A typical mesh resolving the boundary layer properly involves about 1 million nodes. This type of simulation and size model has been validated on several automotive engine cooling fan configurations with both integral performances and detailed flow measurements (Coggiola *et al.* 1998; Neal *et al.* 2001). A similar setup has been used for the electronic fan with rescaled dimensions of the blocks: the computational domain upstream of the fan is $4R_f$ long, and has a radius of $3R_f$; the computational domain downstream of the fan is $6R_f$ long and has a radius of $4R_f$. The computational grid on both rotating machines consists of a structured mesh upstream and downstream of the fan blade. However, the electronic cooling fan blade itself and its close surroundings are meshed using an unstructured grid, meeting the quality requirement of Fluent™. The tetrahedral grid over the fan blade is relatively coarse and does not yet fully resolve the boundary layer.

Only the automotive fan systems involve a complete compression stage in the present study. The influence of the struts in the electronic cooling unit has thus far been neglected. Both the next generation of long efficient stators (Moreau & Bakir 2003) and the more classical short stators (Moreau & Bakir 2002) are associated with the above ultraslim fans. A topological simplification has been made for the actual fan systems to limit the three-dimensional model size to a single blade passage. Firstly, a 9 rotor blades and 9

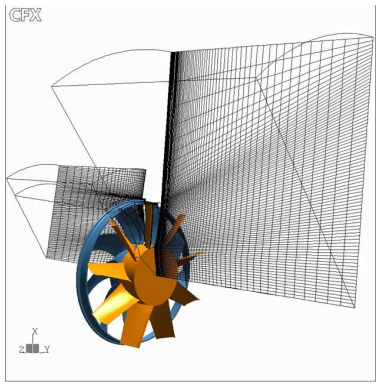

(a) Engine cooling fan system and rotor-stator grid topology

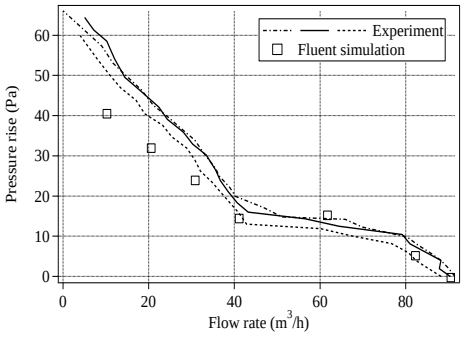

(b) Performance curve of an electronic cooling fan: lines, experimental data; symbols, Fluent simulation

FIGURE 2. *Steady state simulations.*

stator blades (1-1) model has been simulated instead of the actual 10 stator vanes of the 320 mm fan system. This leads to an angular pitch error of 11%. Secondly, a 9 rotor blades and 18 stator blades (1-2) model has been simulated instead of the actual 19 stator vanes of the 380 mm fan system. This yields an angular pitch error of 5.6%. As quoted by Moreau & Bakir (2003), this may not be as serious as in the turbine case of Arnone & Pacciani (1996), where it led to a premature flow choke. In fact the systematic detailed cascade study of Caro (2003) did not show any significant difference for similar angular pitch error in low-speed engine cooling applications. The recent full three-dimensional simulations of both systems by Moreau *et al.* (2005, 2007) suggest that the lower solidity (chord over pitch ratio) in the numerical model may cause a slight under-turning of the stators and consequently a lower overall mean pressure rise through the stage. The rotor-stator grid topology corresponds to the latest evolution of the automatic grid template used for the stator design: one-to-one periodicity is enforced and the wake no longer hits any grid corner. This not only prevented the diffusion of the rotor wakes and enhanced the rotor-stator interaction. It also significantly reduced the RAM required for this type of simulation with CFX-TASCflow™. The overall grid size has been deliberately kept below 1 million grid nodes per blade passage (enough for the spatial resolution) to keep the post-processing tractable and to allow a full-time convergence study. The resulting grid topology in a meridional plane is shown in Fig. 2a.

For all simulations, the multiple frame of reference capability of both commercial codes is used: the blocks close to the blades are put in the rotational reference frame and the inlet and the outlet are kept in the stationary frame. A mass flow rate is imposed at the inlet, a pressure outlet is set at the outflow. No-slip conditions in the proper reference frames are imposed on the solid walls. Periodic boundary conditions are used on the sides of the blade passages.

3.2. *Steady results*

The incompressible, highly rotational and three-dimensional flow field in the above fan systems is described by the three-dimensional turbulent RANS equations with a two-

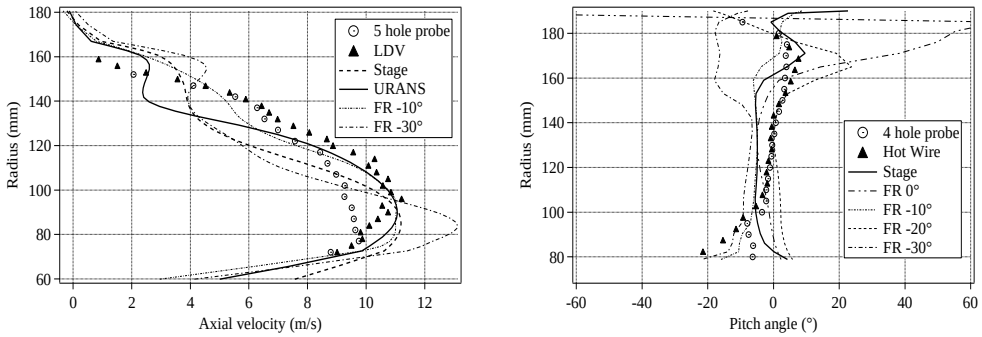

(a) Mean axial velocity 41 mm downstream of the 320 mm fan system

(b) Pitch angle at 33 mm downstream of the 380 mm fan system

FIGURE 3. *Validation of engine cooling fan systems simulations.*

equation turbulence model as a closure. The more stable realizable k-ϵ model is used in the electronic cooling fan simulations with Fluent™. Enhanced wall boundary conditions with pressure gradient effects are also applied on the blade to account for the relative coarse grids. The k-ω SST model is used for the CFX-TASCflow™ simulations of the engine cooling fans on the finer grids mentioned above. The resulting set of conservative equations are discretized with second-order upwind schemes for the convective term, and second-order central differences for all other spatial discretizations. In Fluent™, the pressure-velocity coupling is achieved through the SIMPLEC scheme. Double precision is used in all simulations.

A comparison between experimental results and the simulations of the computer fan is shown in Fig. 2b. The three experimental lines correspond to three different tests on three different samples of the same fan model. The experimental results show the variation in the experiments between the different fan samples. The simulations capture the trend of the measured fan curve to satisfactory agreement. The numerical free flow condition (zero pressure rise) agrees well with all measured data. The simulations also predict the observed plateau in the fan curve. At lower flow rates, the increasing difference between the measured values and the numerical results can be attributed to the grid coarseness, which cannot capture the tip clearance flow and the on-start of suction side flow separations correctly.

Two types of boundary conditions have been applied at the rotor/stator interface: a frozen-rotor (FR) generalized grid interface at various angular positions of the rotor relative to the stator (labeled 0°, -10°, -20°, and -30° in Fig. 3), and a mixed-plane (Stage) condition. Details of the simulations on the selected fan systems can be found in Moreau *et al.* (2005, 2007). For both configurations, the stage solution was found to yield the most accurate mean flow when compared to the frozen-rotor results (see Fig. 3). Most of the frozen-rotor solutions underestimate the pressure load on both blades and can yield spurious unphysical solutions compared to the unsteady solutions shown in the next section. The stage solution is thus chosen as the initial solution for the unsteady simulations.

These steady solutions provide the mean inlet flow conditions (velocity and incidence)

and the boundary layer parameters (displacement thickness and wall shear stress) that are used in the strip theory for the broadband noise prediction presented below.

3.3. *Unsteady results*

The unsteady rotor/stator simulations are also carried out with CFX-TASCflow™ for one rotor blade and one or two stator vane passages. The low-speed highly rotational flow is again modeled by the RANS equations but in a time-dependent fashion. The resulting URANS equations are discretized by a second order implicit scheme in time with a dual time-stepping approach. The fully time-converged simulation on the 320 mm fan system involves 64 iterations per blade passing period (BPP) with 20 pseudo-time steady-state solutions for each physical iteration. Ten cycles are also computed. For the 380 mm fan system, only 16 iterations per BPP have been achieved so far with the same number of pseudo-time steps. The simulations have converged to similar accuracy both in space and time. The resulting integral pressure rise with flow rate for both fan systems was found to compare favorably with the experimental measurements (Moreau *et al.* 2005, 2007). Similarly, for the 320 mm fan system, the axial and tangential velocity profiles 41 mm downstream of the stator vanes were shown to lie within the experimental data spread found in the five-hole and LDV measurements (see Fig. 3a). Only the radial component was found to be significantly underestimated at the hub, which could be explained by the lack of fan ribs in the numerical simulation. These ribs act as centrifugal pumps that generate a strong flow suction through the electrical motor.

As shown in cascade simulations by Moreau *et al.* (2002), the interaction between the rotor wake and the stator leading-edge is the dominant unsteady mechanism. In addition, the large vortical structure developing in the rotor tip region is the second major unsteady mechanism. The latter fully accounts for the larger unsteadiness found in the rotor compared to the previous cascade simulations. The rotor pressure fluctuations now represent about 10% of the mean load. The former contributes to the large fluctuations seen at the stator leading-edge. As in the cascade, the level of pressure fluctuations is as high as for 30% to 40% of the mean load. Additional unsteady secondary flow patterns are also observed on the stator blade both at the leading and trailing-edges. Full details of this simulation have been recently presented by Moreau *et al.* (2005). The wall pressure fluctuations on either the rotor or the stator blades, shown in Fig. 4a and b at the rotor tip at different fractions of the blade passing period T, are used to perform the acoustic analogy predictions that highlight the contribution of the different stage elements to the acoustic energy. The pressure values at all surface grid nodes at all time steps are used in the noise simulation.

4. Acoustic simulations

4.1. *Tonal noise model and results*

The rotor-stator noise prediction code *Foxhawk* developed by Casalino (2003) is used for the present study. Its formulation is based on the retarded-time penetrable FWH formulation of Di Francescantonio (1997) and Brentner & Farassat (1998), translated into a forward-time formulation for moving observers. For the present low-speed fans ($M \ll 1$), only the thickness (subscript T) and loading noise (subscript L) are calculated and the quadrupole noise is ignored. For a fixed observer at $\vec{x} = (x_1, x_2, x_3) = (x_i)$, this yields the following expressions for the far field acoustic pressure:

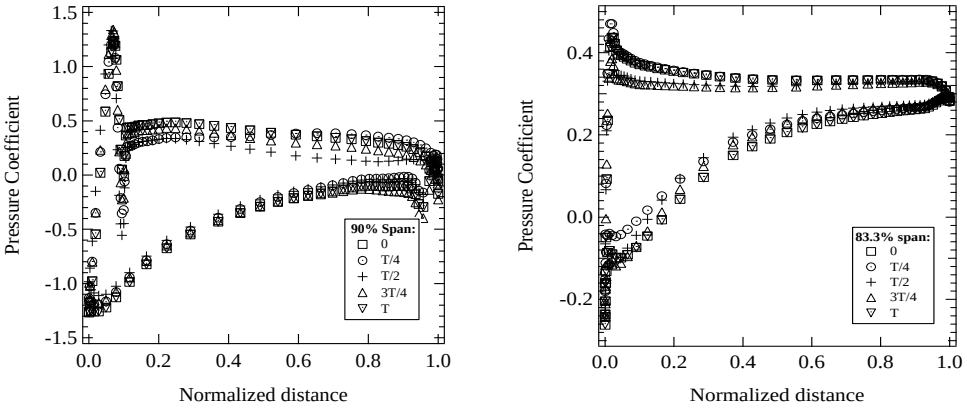

(a) Rotor wall pressure distribution at the tip of the 320 mm fan system

(b) Stator wall pressure distribution at the rotor tip of the 320 mm fan system

FIGURE 4. *Tonal noise sources.*

Thickness noise

$$4\pi\, p'_T(\vec{x},t) = \int_S \left[\frac{\rho_0 \left(\dot{U}_n + U_{\dot{n}}\right)}{r\left(1-M_r\right)^2}\right]_{\text{ret}} \mathrm{d}S + \int_S \left[\frac{\rho_0\, U_n \left(r\dot{M}_r + c_0\left(M_r - M^2\right)\right)}{r^2\left(1-M_r\right)^3}\right]_{\text{ret}} \mathrm{d}S \quad (4.1)$$

where r is the source-to-observer distance, ρ_0 the undisturbed fluid density and c_0 the speed of sound. $\vec{M}$ of magnitude M is the Mach number vector of a source point on the blade surface S, which moves with an outward normal velocity U_n. The dotted quantities denote time derivative with respect to the source time τ. M_r is the relative Mach number, i.e., the projection of $\vec{M}$ in the observer's direction.

Loading noise

$$\begin{aligned} 4\pi\, p'_L(\vec{x},t) = {} & \frac{1}{c_0}\int_S \left[\frac{\dot{F}_r}{r\left(1-M_r\right)^2}\right]_{\text{ret}} \mathrm{d}S + \int_S \left[\frac{F_r - F_M}{r^2\left(1-M_r\right)^2}\right]_{\text{ret}} \mathrm{d}S \\ & + \frac{1}{c_0}\int_S \left[\frac{F_r\left(r\dot{M}_r + c_0\left(M_r - M^2\right)\right)}{r^2\left(1-M_r\right)^3}\right]_{\text{ret}} \mathrm{d}S \end{aligned} \quad (4.2)$$

where $\vec{F}$ is the pressure force acting on the surface S. F_M is this force projected in the source movement direction.

Foxhawk takes advantage of the forward-time formulation by enabling concurrent flow/noise simulations. For the sake of the present work the code is only used to post-process transient wall pressure fields extracted from CFX-TASCflow™ databases built previously. Only linear effects due to the blade thickness and loading are therefore computed. Nonlinear volume quadrupoles are neglected on the basis of low blade tip Mach number. Integrations on rotating and fixed elements can be carried out independently, allowing a separation of the rotor and stator noise contributions. For a single blade, the integration surface consists of 24,120 elements for the 320 mm fan system.

Transient CFD data covering a blade passage (64 multi-block structured files for the

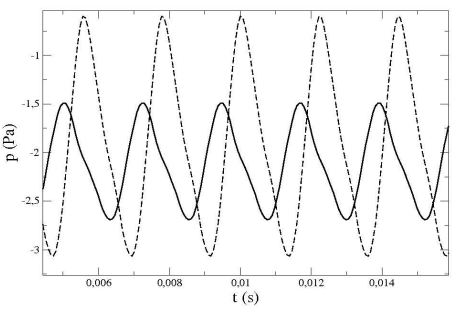

(a) Acoustic pressure signals of the 320 mm fan system: comparison between a 9/9 and a 9/10 configuration

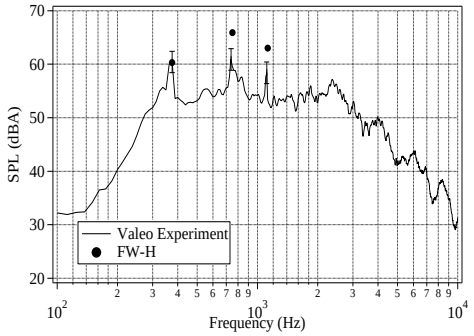

(b) Sound pressure level of the 380 mm fan system: comparison between module measurement and *Foxhawk* predictions

FIGURE 5. *Tonal noise in engine cooling fan systems.*

320 mm fan system and currently only 16 for the 380 mm fan system) are cyclically imported in order to simulate several blade passages. The 320 mm fan rotation frequency is 50 Hz, corresponding to a blade passing frequency f_{NB} (BPF) of 450 Hz. The 380 mm fan rotation frequency is 41.6 Hz, corresponding to a BPF of 375 Hz. The periodic B-blades configuration is automatically generated by *Foxhawk* before integrations. The actual blade counts ($B^{\mathrm{rotor}} = 9$ and $B^{\mathrm{stator}} = 10$ for the 320 mm fan system and $B^{\mathrm{rotor}} = 9$ and $B^{\mathrm{stator}} = 19$ for the 380 mm fan system) are automatically reconstructed by *Foxhawk*. This is made by forcing the following time lag for the i-th blade:

$$\tau_i = (i-1)\,\frac{\mathrm{sgn}\,(\Omega)}{f_{\mathrm{NB}}}\,\frac{B^{\mathrm{stator}} - B^{\mathrm{rotor}}}{B^{\mathrm{stator}}} \tag{4.3}$$

into the forward-time formula. This expression used for both the rotor and the stator blades accounts exactly for a uniform circumferential blade distribution.

The acoustic signals are computed at several microphones arranged on a spherical grid of radius 1 m. We presently focus on the direction along the rotational axis in front of the fan system. Fig. 5a shows that, as expected, a significant decrease in tonal noise is achieved by moving from the same number of rotor and stator blades to vanes that are prime numbers between them. Fig. 5b then shows that the tonal prediction is close to the module measurements up to the second harmonics of the fundamental tone on the 380 mm fan system. Similar results are found for the 320 mm fan system tonal noise.

4.2. *Broadband noise model and results*

For the broadband noise prediction, the main limitation comes from our capability to predict the noise sources accurately within a reasonable computational time. Indeed, a first Large-Eddy Simulation (LES) of the flow over the Valeo CD airfoil used in the above fan systems (Wang *et al.* 2004) showed that a high quality and fine grid (5.1 million nodes) was necessary to achieve numerical stability and yield comparable streamwise and spanwise wall pressure statistics to those measured experimentally. The extension of this body-fitted single block structured mesh to a fan blade with reasonable aspect ratios and tip and hub resolution would require a grid size beyond 500 million nodes.

A realistic automotive engine cooling fan also involves a complex blade geometry with a large variation of blade twist (stagger angle) and rapidly varying blade sweep and rake (highly bowed blades), which makes it hard to design a high quality single block structured grid over the entire blade span. Moreover, the tip clearance involves a much more complex labyrinth than the one considered by You *et al.* (2004), making a local structured body-fitted grid hard to design. Because of this, several unstructured grid topologies have been tested for the CD airfoil by Moreau *et al.* (2006). The LES on these grids will guide us for the future full LES on the complete fan blade. Meanwhile, a simpler approach is considered here, which splits the fan into several radial strips treated as independent airfoils instantaneously in rectilinear motion. The spanwise extent of each strip should be at least the spanwise coherence length of the noise source field.

Acoustic specifications on engine cooling fan systems involve measuring the sound pressure level of a puller fan system (pulling air through the heat exchanger) mounted on a stack of heat exchanger in a semi-anechoic chamber. To account for two possible broadband noise sources in this engine cooling module experimental setup, both the scattering of wall pressure fluctuations at the fan blade trailing-edge (trailing-edge noise) and the scattering of impinging turbulent velocity fluctutations shed by the heat exchanger cores at the fan blade leading-edge (leading-edge noise) are simulated.

The trailing-edge noise formulation initially developed by Amiet (1976) and extended by Roger & Moreau (2005) is reviewed in Moreau *et al.* (2006). It yields the following predicted sound field for low Mach number, $M = U/c_0$, and in the midspan plane, at a given observer location $\vec{x} = (x_1, x_2, 0) = (R, \theta)$ and for a given radian frequency ω (or wavenumber k):

$$S_{pp}^{TE}(\vec{x}, \omega) \;=\; \left(\frac{\sin\theta}{2\,\pi\,R}\right)^2 (k\,c)^2\,\frac{L}{2}\,|I|^2\,\Phi_{pp}(\omega)\,l_y(\omega) \tag{4.4}$$

where Φ_{pp} is the power spectral density (PSD) and $l_y(\omega)$ a spanwise correlation length of the wall pressure fluctuations near the trailing-edge. The radiation integral I is given by Roger & Moreau (2005).

The standard Schwarzschild's solution, which yielded Eq. 4.4 for the trailing-edge noise, was first proposed by Amiet (1975) to handle the problem of the noise from turbulence impinging on an airfoil. It is derived from a generalization obtained by Amiet of the result based on unsteady aerodynamic theories by Adamczyk (1974). The resulting radiated sound field at low Mach numbers at a given observer position in the midspan plane $\vec{x} = (x_1, x_2, 0) = (R, \theta)$ then reads

$$S_{pp}^{LE}(\vec{x}, \omega) = \left(\frac{\rho_0\,U\,\sin\theta}{2\,R}\right)^2 (k\,c)^2\,\frac{L}{2}\,|\mathcal{L}|^2\,\Phi_{ww}(\omega)\,l_y(\omega) \tag{4.5}$$

where Φ_{ww} is the PSD of the vertical velocity fluctuations, $l_y(\omega)$ a cross-correlation length of the velocity fluctuations impinging on the airfoil, and $\mathcal{L}$ the generalized airfoil response function involving the free stream velocity as a parameter.

The above airfoil acoustic models are then extended to a rotating frame by applying them to each blade segment. As an isolated airfoil, a rotating blade segment locally exhibit attached, partially or fully separated boundary layers characterized by well defined wall pressure statistics. It also faces well defined velocity statistics of the incoming turbulence. Therefore the transfer functions from single-airfoil theories can be applied to predict the noise radiated by a complete fan in the far field, provided that the required information

is available at different radii. The main idea is that the circular motion can be considered locally as tangential to an equivalent translating motion, for which Eqs. (4.4) and (4.5) hold. This is only true for sound frequencies higher than the rotational frequency. Initially developed for high-speed blades of model helicopter rotors in the wind-tunnel tests by Paterson & Amiet (1979) and Schlinker & Amiet (1981), the analysis presented here is valid for low Mach number fans, operating in a medium at rest.

Let (x_1, x_2, x_3) be the instantaneous coordinates of the observer in a reference frame attached to a blade segment at angle Ψ. At the corresponding instant the surrounding fluid is moving with respect to the blade with the velocity U induced by the rotation. This velocity is assumed parallel to the chord line according to the weakly loaded airfoil assumption in the linearised theory. Sound propagates toward the observer according to the convected Helmholtz equation expressed in the reference frame (x_1, x_2, x_3). The solution is given exactly by the single-airfoil formulae provided that the convection effects are negligible on the sound propagation. This is particularly the case for the present low-speed fan applications.

Since the blade moves with respect to the observer, the instantaneous emitted frequency $\omega_e(\Psi)$ at current position $\Psi = \Omega t$ corresponding to the given frequency received by the observer ω is determined by the Doppler factor, according to the formula

$$\frac{\omega_e(\Psi)}{\omega} \;=\; 1 \,+\, M\,\sin\Theta\;\sin\Psi \;=\; 1 - M_r \tag{4.6}$$

where $M = \Omega R/c_0$ is the rotational Mach number at radius R for angular velocity Ω. The sound received at frequency ω is produced by sources on the rotating blade segment having different frequencies depending on their angular position. The resulting spectrum must be calculated by averaging over all possible angular locations of the blade segment and by weighting with the Doppler ratio. This yields the following far field noise PSD for a fan with B blades:

$$S_{pp}(\vec{x},\omega) \;=\; \frac{B}{2\,\pi}\;\int_0^{2\pi}\frac{\omega_e(\Psi)}{\omega}\;S^{\Psi}_{pp}(\vec{x},\omega_e)\;\,d\Psi \tag{4.7}$$

in which $S^{\Psi}_{pp}(\vec{x},\omega_e)$ denotes the total noise spectrum coming from both noise mechanisms, which would be radiated from the current blade segment at angle Ψ ignoring the Doppler frequency shift. $S^{\Psi}_{pp}(\vec{x},\omega_e)$ is precisely what is provided by the single-airfoil formulae.

The above strip theory demonstrated by Eq. (4.7) was first validated on the helicopter rotor test case of Schlinker & Amiet (1981). The model predictions are here compared to the above module measurements on the 380 mm fan system. Figure 6a compares the trailing-edge noise results using the available experimental Φ_{pp}, l_y and U_c values at two flow regimes possibly met in the fan, namely attached and nearly separated turbulent boundary layers, repeated over the whole blade span. Both trailing-edge noise calculations collapse at high frequencies as expected from the wall pressure spectra and match well with the measured spectrum for frequencies beyond 4 kHz. The result for highly loaded blades ($\alpha_g = 15°$) also suggests that some of the medium frequency range (between 1 and 4 kHz) could be explained by larger angles of attack on the tip sections than expected from inlet speed triangles due to the tip clearance recirculation flow in the actual production module configuration. Figure 6b incorporates the turbulence-interaction noise mechanism into the comparison with the module measurements. The measured velocity statistics corresponding to a 4% turbulence intensity behind a heat exchanger is also applied over

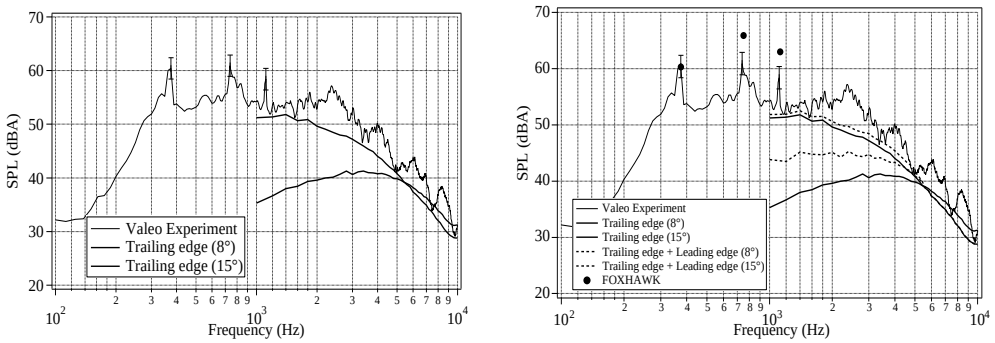

(a) Sound pressure level of the 380 mm fan system: comparison between module measurement and trailing-edge noise predictions

(b) Sound pressure level of the 380 mm fan system: comparison between module measurement and full predictions (tonal+trailing-edge+leading-edge noise)

FIGURE 6. *Tonal and broadband noise in engine cooling fan systems.*

the whole blade span. This corresponds to a heat exchanger in average proximity to the fan system as used in the experiment. Therefore a significant contribution of the leading-edge noise might be expected between 1 and 4 kHz. In both figures, the observed experimental humps are not found in the simulations, which might be due to additional noise mechanisms not accounted for in the present model, such as tip flow effects or vortex shedding.

5. Conclusions

The present study represents the first attempt at computing the complete noise spectrum of a low-speed fan such as those found in automotive engine cooling or electronic cooling modules.

The tonal noise prediction relies on the Ffowcs Williams-Hawkings acoustic analogy, using the pressure fluctuations on the blades computed from detailed Unsteady Reynolds-Averaged Navier-Stokes simulations (URANS). The incompressible URANS simulations were performed on two different automotive engine cooling fan systems involving ultra-compact fans associated with both short and long stator vanes. These simulations have been validated by comparisons with overall performances as well as detailed hot-wire, five-hole probe and laser Doppler anemometry in the fan system wakes.

The broadband noise calculation for a full rotating machine in open space relies on a strip theory, which represents the fan blade as a series of independent airfoils in translation at the local relative velocity. The noise sources are assumed to be uncorrelated and similar to those on a stationary fan airfoil embedded in the jet flow of anechoic wind tunnels. The latter experiments provide the necessary experimental parameters for the two noise mechanisms considered here: the turbulence-interaction noise or leading-edge noise that arises from the heat exchanger turbulence ingested by the fan systems, and the trailing-edge noise or self-noise that is caused by the diffraction of pressure fluctuations underneath the blade boundary layers at the trailing-edge. The sound predictions for these two mechanisms are based on the extended Amiet's theory.

The overall agreement of the combined acoustic predictions with the measurement

on an automotive engine cooling module suggests that URANS calculations can yield accurate noise sources for tonal noise and that the two suggested broadband noise mechanisms co-exist: the turbulence-interaction noise at low and medium frequencies, and the trailing-edge noise at high frequencies beyond 4 kHz.

Finally, the forward-time formulation of the Ffowcs Williams-Hawkings equation leads to the following perspective: the acoustic pressure at the observer location is computed simultaneously as the unsteady flow simulation evolves. The time needed to achieve a converged acoustic signature may then be estimated based on which the URANS calculations for tonal noise prediction can be reduced significantly. The same methodology is applicable to the electronic cooling chassis fan.

Acknowledgments

The authors would like to thank the P2/GMV team in La Verrière R&D center of Valeo Thermal Systems for their technical support and Delta Electronics Inc. for providing us with an electronic cooling fan geometry.

REFERENCES

Adamczyk, J. J. 1974 The passage of an infinite swept airfoil through an oblique gust. *NASA CR 2395*.

Amiet, R. K. 1975 Acoustic radiation from an airfoil in a turbulent stream. *J. Sound Vib.* **41**(4), 407–420.

Amiet, R. K. 1976 Noise due to turbulent flow past a trailing edge. *J. Sound Vib.* **47**(3), 387–393.

Arnone, A. & Pacciani, R. 1996 Rotor-stator interaction analysis using the Navier-Stokes equations and a multigrid method. *J. Turbomachinery* **118**, 679–689.

Caro, S. & Moreau, S. 2000 Aeroacoustic modeling of low pressure axial flow fans. *AIAA Paper 2000-2094*, 6^{th} AIAA/CEAS Aeroacoustics Conference, Lahaina, Hawaii.

Caro, S. 2003 Contribution à la prévision du bruit d´origine aérodynamique d´un ventilateur de refroidissement. *PhD Thesis*, Ecole Centrale de Lyon, France.

Casalino, D. 2003 An advanced time approach for acoustic analogy predictions. *J. Sound Vib.* **261**(4), 583–612.

Coggiola, E., Dessale, B., Moreau, S. & Broberg, R. 1998 On the use of CFD in the automotive engine cooling fan system design. *AIAA Paper 98-0772*, 36^{th} AIAA Aerospace Sciences Meeting and Exhibit, Reno, Nevada.

Brentner, K. S. & Farassat, F. 1998 Analytical comparison of the acoustic analogy and Kirchhoff formulation for moving surfaces. *AIAA J.* **36**(8), 1379–1386.

Di Francescantonio, P. 1997 A new boundary integral formulation for the prediction of sound radiation. *J. Sound Vib.* **202**(4), 491–509.

Henner, M., Kessaci, S. & Moreau, S. 2002 Latest improvements of CFD models of engine cooling axial fans systems. *SAE paper 2002HX-36*, SAE 2002 World Congress, Detroit, Michigan.

Huang, L. 2003 Characterizing computer cooling fan noise. *J. Acoust. Soc. Am.* **114**, 3189–3200.

Hubbard, H. H. & Shepherd, K. P. 1991 Aeroacoustics of large wind turbines. *J. Acoust. Soc. Am.* **89**, 2495–2507.

Moreau, S. & Bakir, F. 2002 Efficient stator design for automotive engine cooling fan systems. *FEDSM02-31318 paper*, ASME 2002 Fluids Engineering Division Summer Meeting, Montreal, Canada.

Moreau, S., Aubert, S. & Ferrand, P. 2002 Detailed 2D unsteady rotor-stator interaction in automotive engine cooling fan systems. *FEDSM2002-31347 paper*, ASME 2002 Fluids Engineering Division Summer Meeting, Montreal, Canada.

Moreau, S. & Bakir, F. 2003 Detailed study of an efficient small diameter automotive engine cooling fan systems. *FEDSM2003-45117 paper*, ASME 2003 Fluids Engineering Division Summer Meeting, Honolulu, Hawaii.

Moreau, S., Henner, M. & Neal, D. 2005 Detailed 3D unsteady rotor-stator interaction in automotive engine cooling fan systems. 6^{th} European Conference on Turbomachinery Fluid Dynamics and Thermodynamics, Lille, France.

Moreau, S., Neal, D., Khalighi, Y., Wang, M. & Iaccarino, G. 2004 LES prediction of wall pressure spectra on a low speed airfoil. *Proceedings of the Summer Program 2006*, Center for Turbulence Research, Stanford Univ./NASA Ames.

Moreau, S., Henner, M., Brouckaert, J.F. & Neal, D. 2007 Numerical and experimental investigation of rotor-stator interaction in automotive engine cooling fan systems. 7^{th} European Conference on Turbomachinery Fluid Dynamics and Thermodynamics, Athens, Greece.

Neal, D., Moreau, S., Henner, M. & Foss, J. 2001 Evaluating CFD models of axial fans by comparisons with phase-averaged experimental data. *VTMS5-01-89 Paper*, 5^{th} Vehicle Thermal Management Systems Conference, Nashville, Tennessee.

Paterson, R. W. & Amiet, R./ K. 1979 Noise of a model helicopter rotor due to ingestion of turbulence. *NASA CR 3213*.

Roger, M. & Moreau, S. 2004 Trailing edge noise measurements and prediction for a subsonic loaded fan blade. *AIAA J.* **42**(3), 536–544.

Roger, M. & Moreau, S. 2004 Back-scattering correction and further extensions of Amiet's trailing edge noise model. Part 1: theory. *J. Sound Vib.* **286**(3), 477–506.

Schlinker, R. H. & Amiet, R./ K. 1981 Helicopter trailing edge noise. *NASA CR 3470*.

Wang, M., Moreau, S., Iaccarino, G. & Roger, M. 2004 LES prediction of wall pressure spectra on a low speed airfoil. *Annual Research Briefs-2004*, Center for Turbulence Research, Stanford Univ./NASA Ames.

Wright, S.E. 1976 The acoustic spectrum of axial flow machines. *J. Sound Vib.* **45**(2), 165–223.

You, D., Mittal, M., Wang, M. & Moin, P. 2004 Computational methodology for large-eddy simulation of tip-clearance flows. *AIAA J.* **42**(2), 271–279.